Inorganic Chemistry

Article

pubs.acs.org/IC

Valence Tautomeric Transitions of Three One-Dimensional Cobalt Complexes

Xiang-Yi Chen, Rong-Jia Wei, Lan-Sun Zheng, and Jun Tao*

State Key Laboratory of Physical Chemistry of Solid Surfaces and Department of Chemistry, College of Chemistry and Chemical Engineering, Xiamen University, Xiamen 361005, People's Republic of China

Supporting Information

ABSTRACT: Three novel complexes, namely, $[Co^{III}(3,5\text{-DBCat})(3,5\text{-DBSq})(bpe)]\cdot 2CH_3CN\cdot 2H_2O$ (**1**·*S*), $[Co^{III}(3,5\text{-DBCat})(3,5\text{-DBSq})(azpy)]\cdot 2CH_3CN\cdot 2H_2O$ (**2**·*S*), and $[Co^{II}(3,5\text{-DBSq})_2(bpb)][Co^{III}(3,5\text{-DBCat})(3,5\text{-DBSq})(bpb)]_{0.5}\cdot 2CH_3CN\cdot 2H_2O$ (**3**·*S*), were synthesized and characterized by valence tautomeric (VT) X-ray diffraction and magnetic measurements [where $3,5\text{-DBCatH}_2$ = 3,5-di-*tert*-butyl-catechol, 3,5-DBSqH = 3,5-di-*tert*-butyl-semiquinone, bpe = *trans*-bis(4-pyridyl)ethylene, azpy = *trans*-4,4′-azopyridine, and bpb = 1,4-bis(4-pyridyl)-benzene]. The three complexes have similar one-dimensional chain structure building from bidentate-bridging pyridine ligands and planar 3,5-DBCat/3,5-DBSq-fixed $Co^{II/III}$ entities. Complexes **1**·*S* and **2**·*S* could retain the crystallinity during desolvation, and the crystal structures of **1** and **2** were therefore able to be determined. Only when **1**·*S* and **2**·*S* desolvated above 310 K did the magnetic susceptibilities × temperatures values of the two complexes rise sharply, and then thermally induced complete, one-step VT transitions for **1** and **2** were available and repeatable. Complex **3**·*S* showed an incomplete, one-step VT transition independent of solvent molecules. Among these complexes, only **1** was sensitive to photoexcitation at low temperature, its photoinduced metastable state relaxed with temperature-independent behavior at low temperature range (5−10 K) and with thermally assisted behavior at high temperature range (above 20 K), respectively.

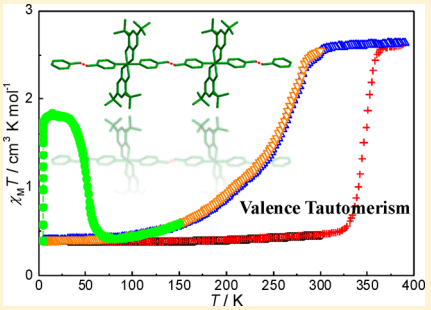

INTRODUCTION

Electronically labile metal complexes that can switch between two or more distinguishable electronic configurations are often susceptible to external stimuli such as temperature, pressure, light irradiation, or magnetic field.[1−7] Since the switch is usually associated with large variations in optical and/or magnetic properties, such species represent an important goal in the miniaturization of electronic devices for display, sensing, and data storage.[8−11] As one of the most interesting electronically labile metal complexes, valence tautomeric (VT) complexes involving intramolecular electron transfer between metal center and redox-active ligand as well as simultaneous spin-state crossover of the metal center are attracting considerable interest.[12,13] For instance, several studies have been concentrated on the mononuclear cobalt−dioxolene VT complexes using chelate pyridyl-based ligands to fulfill the coordination spheres.[14−19] In these complexes, when the antibonding orbitals (e_g orbitals) of metal ion are energetically close to the frontier orbitals of dioxolene ligand, an intramolecular two-step redox reaction-induced VT transition can take place.[12,16,20−22]

Currently, most cobalt-based VT complexes are mononuclear,[7,14,16,19,23−25] while one-dimensional (1D) cobalt-based VT complexes are rather rare (Scheme 1a). The first such 1D VT complex, $[Co^{III}(3,6\text{-DBCat})(3,6\text{-DBSq})(pz)]$ ($3,6\text{-DBCatH}_2$ = 3,6-di-*tert*-butyl-catechol, 3,6-DBSqH = 3,5-di-*tert*-butyl-semiquinone, pz = pyrazine), showed interesting photomechanical behavior that was associated with its 1D structure bridged by pyrazine and structural distortion.[7,26] When the crystal was illuminated, light-induced change in charge distribution occurred—known as ligand-to-metal charge transfer (LMCT)—so that the complex unit along the chain

Scheme 1. Bridging Ligands[a]

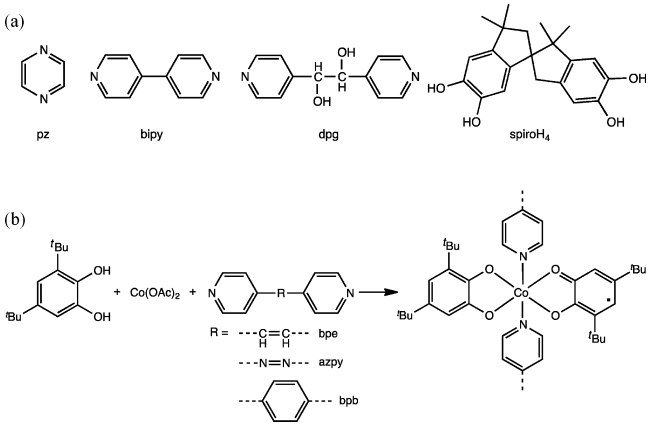

[a](a) In reported 1D cobalt VT complexes. (b) Used to synthesize the title complexes as well as the synthetic procedure.

Received: October 8, 2014
Published: November 25, 2014

   dx.doi.org/10.1021/ic502471v | *Inorg. Chem.* 2014, 53, 13212−13219

Table 1a. Crystal Data and Structural Refinement Parameters for 1·*S*−3·*S*

complex	**1**·*S* at 100 K	**1**·*S* at 300 K	**2**·*S* at 100 K	**2**·*S* at 300 K	**3**·*S* at 100 K	**3**·*S* at 300 K
formula	$C_{44}H_{60}CoN_4O_6$		$C_{42}H_{58}CoN_6O_6$		$C_{70}H_{88}Co_{1.5}N_5O_8$	
M_r/g mol^{-1}	799.89		801.87		1215.85	
crystal system	triclinic		triclinic		triclinic	
space group	$P\bar{1}$		$P\bar{1}$		$P\bar{1}$	
a/Å	8.7027(8)	8.7245(11)	8.5902(15)	8.6043(6)	15.1825(12)	15.2442(15)
b/Å	11.1040(9)	11.1242(7)	11.072(2)	11.1246(5)	15.2340(11)	15.2808(8)
c/Å	11.7255(11)	11.7352(9)	11.686(2)	11.7325(8)	16.6588(14)	16.9964(10)
α/deg	104.665(7)	104.632(5)	103.247(6)	103.208(5)	101.638(7)	100.843(5)
β/deg	98.560(8)	98.382(7)	97.139(6)	96.996(6)	96.941(7)	99.057(8)
γ/deg	97.200(7)	97.482(6)	99.591(5)	100.004(5)	101.291(6)	100.687(7)
V/Å^3	1068.11(17)	1073.51(18)	1051.4(3)	1061.31(11)	3648.8(5)	3744.4(5)
Z	1	1	1	1	2	2
D_{calcd}/g cm^{-1}	1.244	1.237	1.266	1.266	1.107	1.078
reflns collected	3227	3618	4813	3599	11122	12385
unique reflns	2621	2832	2187	2942	5373	6219
$F(000)$	427	427	427	427	1295	1295
GOF	0.889	1.043	0.914	1.012	1.024	1.070
$R1^a$ $[I > 2\sigma(I)]$	0.0459	0.0702	0.0683	0.0616	0.0982	0.0944
$wR2^b$ (all data)	0.1438	0.1915	0.2133	0.1704	0.2785	0.2625
CCDC number	1006400	1023735	1006401	1023736	1012420	1017389

$^a R1 = \Sigma||F_0| - |F_c||/\Sigma|F_0|$. $^b wR2 = \{\Sigma[w(F_0^2 - F_c^2)^2]/\Sigma[w(F_0^2)^2]\}^{1/2}$.

direction underwent an elongation of the Co−N bond and thus an anisotropic expansion of the crystal volume. Recently, an interesting VT complex, [Co^{III}(3,5-DBCat)(3,5-DBSq)(bipy)] (bipy = 4,4′-bipyridine),[27] was obtained, which confirmed the strategy of using bridging ligand to achieve functional materials in the nanoparticle-formation process. This complex showed an abrupt VT transition near room temperature. In 2012, we reported a new 1D cobalt VT complex that was synthesized through adopting *meso*-*α*,*β*-di(4-pyridyl)glycol as bridging ligand.[28] Interestingly, it showed not only photoswitchable interconversion between the two tautomers but also a pressure effect on the VT transition. Besides, using bis-bidentate tetraoxolene ligand could also lead to the formation of 1D VT complexes, as exemplified by [Co(L)(spiro)]·3H$_2$O (L = 2,2′-bipyridine or 1,10-phenanthroline, spiroH$_4$ = 3,3,3′,3′-tetramethyl-5,5′,6,6′-tetrahydroxy-1,1′-spirobisindane),[29] which showed time-dependent changes of the magnetic susceptibilities and displayed thermally and photoinduced VT transitions.

Inspired by these results, we think that 1D complexes formed with *exo*-bidentate pyridine ligands and Cat/Sq-fixed Co$^{II/III}$ units may exhibit interesting physical properties associated with VT transitions, and therefore we choose three *exo*-bidentate pyridine ligands (Scheme 1b), namely, *trans*-bis(4-pyridyl)-ethylene (bpe), *trans*-4,4′-azopyridine (azpy), and 1,4-bis(4-pyridyl)benzene (bpb), to synthesize 1D VT complexes. Here, we report the syntheses and crystal structures of three novel 1D complexes and their bridging ligand-, solvent-, temperature-dependent, and light-induced VT properties.

EXPERIMENTAL SECTION

Materials and Physical Measurements. All reagents were obtained from commercial sources and were used as received. Powder X-ray diffraction (PXRD) data were recorded on Panalytical X'pert PRO diffractometer with Cu Kα radiation (λ = 0.154 18 nm, 40.0 kV, 30.0 mA) at room temperature. Elemental analyses for C, H, and N were performed on PerkinElmer 240Q elemental analyzer. IR spectra (KBr pellets) were recorded in the range of 400−4000 cm^{-1} on a Nicolet 5DX spectrophotometer. Magnetic measurements were carried out at a sweeping rate of 1.5 K min^{-1} on a Quantum Design SQUID XL7 magnetometer in the 5−390 K temperature range. Magnetic susceptibilities were calibrated with the sample holder, and diamagnetic corrections were estimated from Pascal's constants. Light irradiation was performed using CNI MBL 532 nm laser (150 mW); the light was introduced into the sample chamber through a hollow sample rod. The 532 nm excitation wavelength was chosen based on the photoirradiation effect of [Co^{III}(3,5-DBCat)(3,5-DBSq)(py)$_2$]/[Co^{II}(3,5-DBSq)$_2$(py)$_2$].[43]

Synthesis. Complexes **1**·*S*, **2**·*S*, and **3**·*S* were synthesized in test tubes by using a method similar to that for the unique two-dimensional VT complex.[30] An aqueous solution (2 mL) of Co(CH$_3$COO)$_2$·4H$_2$O (0.025 g, 0.1 mmol) was put in the bottom of a test tube, and then an acetonitrile solution (10 mL) of 3,5-DBCatH$_2$ (0.022 mg, 0.1 mmol) and a bridging ligand (0.1 mmol; bpe for **1**·*S*, azpy for **2**·*S* and bpb for **3**·*S*, respectively) was carefully layered on. Dark green crystals of **1**·*S*−**3**·*S* suitable for single-crystal XRD analysis were obtained in several weeks. Desolvated crystalline samples **1**−**3** were obtained by heating the as-synthesized **1**·*S*−**3**·*S* (∼100 mg of each) crystals, respectively, in vacuum at 90 °C for 1 h.

*[Co^{III}(3,5-DBCat)(3,5-DBSq)(bpe)]·2CH$_3$CN·2H$_2$O (**1**·S).* Yield ≈ 80%. Anal. Calcd (%) for $C_{44}H_{60}N_4O_6Co$: C, 66.07; H, 7.561; N, 7.004. Found: C, 66.42; H, 7.365; N, 6.525. IR (cm^{-1}): 3438(s), 2954(s), 1610(s), 1575(m), 1506(w), 1458(s), 1437(s), 1411(w), 1385(m), 1355(m), 1284(m), 1244(m), 1201(m), 1093(m), 1066(m), 1024(m), 983(s), 829(w). Anal. Calcd (%) for the desolvated sample **1** ($C_{40}H_{50}N_2O_4Co$): C, 70.47; H, 7.392; N, 4.109. Found: C, 70.19; H, 7.856; N, 4.123.

*[Co^{III}(3,5-DBCat)(3,5-DBSq)(azpy)]·2CH$_3$CN·2H$_2$O (**2**·S).* Yield ≈ 65%. Anal. Calcd (%) for $C_{42}H_{58}N_6O_6Co$: C, 62.91; H, 7.290; N, 10.48. Found: C, 62.62; H, 7.265; N, 10.52. IR (cm^{-1}): 3433(s), 2958(s), 1630(w), 1581(s), 1471(m), 1413(s), 1385(m), 1355(m) 1284(w), 1244(m), 1222(w), 1202(w), 1097(m), 1026(w), 985(m), 906(w), 852(w). Anal. Calcd (%) for the desolvated sample **2** ($C_{38}H_{48}N_4O_4Co$): C, 66.75; H, 7.076; N, 8.194. Found: C, 66.41; H, 7.337; N, 8.123.

*[Co^{II}(3,5-DBSq)$_2$(bpb)][Co^{III}(3,5-DBCat)(3,5-DBSq)(bpb)]$_{0.5}$·2CH$_3$CN·2H$_2$O (**3**·S).* Yield ≈ 70%. Anal. Calcd (%) for $C_{70}H_{88}N_5O_8Co_{1.5}$: C, 69.15; H, 7.295; N, 5.760. Found: C, 68.75; H, 7.431; N, 5.881. IR (cm^{-1}): 3444(m), 3072(w), 2952(s), 1664(w), 1610(s), 1483(s), 1459(s), 1421(w), 1388(w), 1355(m), 1284(m), 1246(m), 1217(m), 1095(w), 1072(m), 1010(w), 985(m), 906(w), 856(w), 835(w), 808(s). Anal. Calcd (%) for the desolvated sample **3**

dx.doi.org/10.1021/ic502471v | Inorg. Chem. 2014, 53, 13212−13219

Table 1b. Crystal Data and Structural Refinement Parameters for 1 and 2

complex	**1** at 100 K	**1** at 300 K	**2** at 100 K	**2** at 300 K
formula	$C_{40}H_{50}CoN_2O_4$		$C_{38}H_{48}CoN_4O_4$	
M_r/g mol^{-1}	681.75		683.73	
crystal system	triclinic		triclinic	
space group	$P\bar{1}$		$P\bar{1}$	
a/Å	8.6772(7)	8.7618(12)	8.5650(10)	8.6922(5)
b/Å	11.0715(8)	11.1934(8)	11.039(2)	11.1186(6)
c/Å	11.6911(10)	11.7919(8)	11.651(3)	11.8325(9)
α/deg	104.675(7)	104.578(6)	103.256(6)	103.138(6)
β/deg	98.570(7)	98.186(9)	97.143(5)	96.916(6)
γ/deg	97.190(8)	97.789(8)	99.588(6)	100.204(5)
V/Å^3	1058.70(16)	1089.97(18)	1042.0(3)	1080.50(12)
Z	1	1	1	1
D_{calcd}/g cm^{-1}	1.069	1.039	1.090	1.051
reflns collected	3163	3623	4736	3591
unique reflns	2561	2847	2147	2937
F(000)	363	363	363	363
GOF	0.948	1.017	1.000	1.043
$R1^a$ [$I > 2\sigma(I)$]	0.0651	0.1051	0.0823	0.0872
$wR2^b$ (all data)	0.1519	0.1999	0.2442	0.2405
CCDC number	1017385	1017386	1017387	1017388

$^a R1 = \Sigma||F_0| - |F_c||/\Sigma|F_0|$. $^b wR2 = \{\Sigma[w(F_0^2 - F_c^2)^2]/\Sigma[w(F_0^2)^2]\}^{1/2}$.

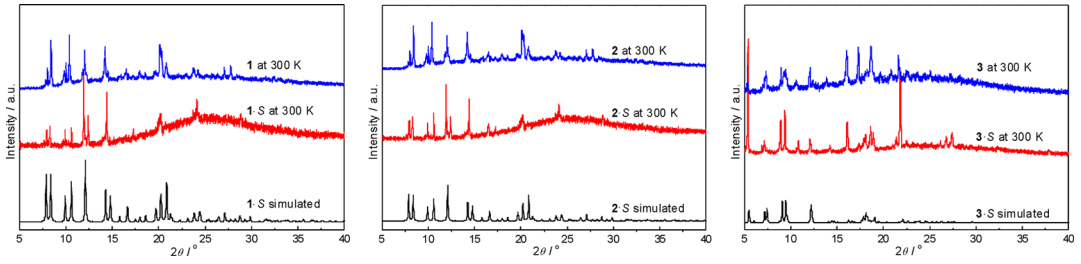

Figure 1. PXRD patterns of the as-synthesized **1**·*S*–**3**·*S* and their desolvated samples.

Table 2a. Selected Bond Lengths [Å] for 1·*S*–3·*S*

1·*S*			**3**·*S*			
bond	100 K	300 K	molecule	bond	100 K	300 K
Co1–O1	1.880(2)	1.877(3)	**Mol1**	Co1–O1	1.858(5)	2.012(10)
Co1–O2	1.884(2)	1.871(3)		Co1–O2	1.868(5)	2.030(9)
Co1–N1	1.939(3)	1.933(3)		Co1–O3	1.901(5)	2.057(9)
O1–C8	1.328(4)	1.327(4)		Co1–O4	1.904(5)	2.048(9)
O2–C7	1.329(4)	1.317(4)		Co1–N1	1.921(6)	2.046(10)
C7–C8	1.420(5)	1.401(6)		Co1–N2	1.933(6)	2.071(11)
				O1–C17	1.343(8)	1.279(14)
	2·*S*			O2–C22	1.335(9)	1.295(13)
bond	100 K	300 K		O3–C31	1.265(9)	1.264(14)
Co1–O1	1.889(3)	1.884(2)		O4–C36	1.299(8)	1.278(15)
Co1–O2	1.880(3)	1.873(2)		C17–C22	1.417(9)	1.454(15)
Co1–N1	1.933(4)	1.957(2)		C31–C36	1.468(10)	1.460(17)
O1–C6	1.341(5)	1.307(4)	**Mol2**	Co2–O5	1.900(5)	1.881(9)
O2–C7	1.332(5)	1.327(4)		Co2–O6	1.885(5)	1.901(8)
C6–C7	1.419(7)	1.406(5)		Co2–N3	1.939(5)	1.971(8)
				O5–C45	1.315(9)	1.347(13)
				O6–C50	1.340(9)	1.317(15)
				C45–C50	1.408(10)	1.424(16)

($C_{66}H_{78}N_3O_6Co_{1.5}$): C, 72.21; H, 7.162; N, 3.828. Found: C, 72.55; H, 7.324; N, 3.914.

X-ray Structure Determination. Single-crystal XRD data were recorded on Agilent SuperNova CCD diffractometer at 100 and 300 K for **1**, **2**, and **1**·*S*–**3**·*S*. The structures were solved by direct methods and refined on F^2 by anisotropic full-matrix least-squares methods using SHELXL-97.[31] All non-hydrogen atoms were refined anisotropically, while hydrogen atoms were generated by the riding mode. The

dx.doi.org/10.1021/ic502471v | *Inorg. Chem.* 2014, 53, 13212–13219

Table 2b. Selected Bond Lengths [Å] for 1 and 2

1			2		
bond	100 K	300 K	bond	100 K	300 K
Co1−O1	1.886(9)	2.042(12)	Co1−O1	1.898(8)	2.018(11)
Co1−O2	1.884(8)	2.071(13)	Co1−O2	1.885(8)	2.014(11)
Co1−N1	1.928(10)	2.128(14)	Co1−N1	1.927(10)	2.075(12)
O1−C8	1.323(12)	1.292(15)	O1−C6	1.333(14)	1.273(16)
O2−C7	1.320(12)	1.274(15)	O2−C7	1.314(13)	1.282(16)
C7−C8	1.400(19)	1.444(18)	C6−C7	1.403(13)	1.443(18)

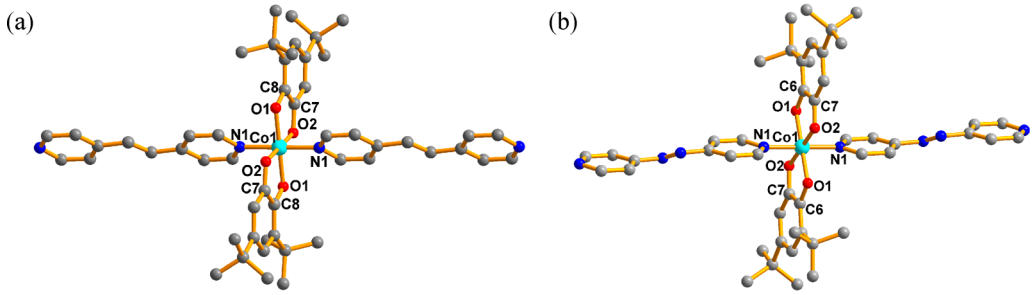

Figure 2. Structural units of **1**·*S* (a) and **2**·*S* (b) shown with selected atom labels. Hydrogen atoms and solvent molecules were omitted for clarity.

solvent molecules in the crystal lattices of **1**·*S* and **2**·*S* could be established by single-crystal structural determination. However, the solvent molecules in **3**·*S* were too disordered to be modeled, so they were determined by elemental and thermogravimetric analyses (Figure S1, Supporting Information), and its 1D structure was handled using the "SQUEEZE" procedure implanted in the PLATON software (see details in Supporting Information).[32] In contrast to **1**·*S* and **2**·*S*, the desolvation of **3**·*S* could not give high-quality crystals of solvent-free **3** to collect single-crystal XRD data. A summary of the crystallographic data and refinement parameters is shown in Tables 1a and 1b. Additional crystallographic information is available in the Supporting Information.

RESULTS AND DISCUSSION

Synthesis. Crystals of **1**·*S*−**3**·*S* were obtained by diffusion method in 20 mL test tubes. The crystal quality was mainly affected by the stoichiometry of reactants and the CH_3CN/H_2O ratio. An amount of 0.05−0.1 mmol of each reactant and overall 15 mL of CH_3CN/H_2O solution (v/v = 5:1) would contribute to high-quality dark green block crystals of **1**·*S*−**3**·*S* with good yield. PXRD studies indicated that the as-synthesized and desolvated samples were phase pure and stable (Figure 1).

Crystal Structures. Structure determinations of **1**·*S*−**3**·*S*, **1**, and **2** were carried out under various temperatures to correlate the spin states of $Co^{II/III}$ centers with structural parameters. Selected bond lengths are summarized in Tables 2a and 2b, and bond angles are shown in Table S1 (Supporting Information).

The asymmetric unit of **1**·*S* contains a Co atom located at an inversion center (i.e., 0.5 occupancy), a half bpe ligand, and a dioxolene ligand. Besides, there are an acetonitrile and a water molecule in the crystal lattice for each asymmetric unit. As shown in Figure 2a, the hexacoordinate Co center lies in a slightly distorted octahedral coordination sphere, which is constituted with two *trans*-disposed pyridyl N atoms from two bpe ligands and four O atoms from two dioxolene ligands. At 100 K, the Co1−O1 and Co1−O2 bond lengths are 1.884(2) Å and 1.880(2) Å, respectively, while the Co1−N1 bond length is 1.939(3) Å, indicating that the Co atom is stabilized in the low-spin (ls) state Co^{III}. Meanwhile, the bond lengths of O1−C8, O2−C7, and C7−C8 are 1.328(4), 1.329(4), and 1.420(5) Å, respectively, which are almost intermediate between those expected for 3,5-$DBCat^{2-}$ and 3,5-$DBSq^{\bullet-}$.[17,30−36] Consequently, the dioxolene ligand is in fact occupied by "half" 3,5-$DBCat^{2-}$ and "half" 3,5-$DBSq^{\bullet-}$, which are delocalized and cannot be distinguished. Therefore, the structural unit at 100 K can be assigned to the ls-Co^{III}−Cat^{2-}-$Sq^{\bullet-}$ electronic configuration.[33−35] While at 300 K, the bond lengths of Co−O, Co−N, O−C, and C7−C8 slightly decrease (<0.02 Å, Table 2a) in comparison to those at 100 K, implying that the 1D structure remains in the ls-Co^{III}−Cat^{2-}-$Sq^{\bullet-}$ state. Thus, the variable-temperature structural studies reveal that **1**·*S* is paramagnetic (free radical $S = 1/2$) and does not display VT transition below room temperature, which is consistent with the magnetic properties (see below).

The desolvated single crystal, **1**, shows the same 1D structure as that of **1**·*S* (Figure 2a). However, its bond distances undergo significant changes upon temperature increase. At 100 K, the Co−O, Co−N, O−C, and C−C distances (Table 2b) are almost identical to those of **1**·*S*, which reveal that **1** should also be in the ls-Co^{III}−Cat^{2-}-$Sq^{\bullet-}$ state. Upon temperature increase to 300 K, The Co−O and Co−N bonds elongate by 0.171 Å (average) and 0.200 Å, respectively, and the C−O bonds shorten from 1.321 Å (average) to 1.283 Å (average). Besides, the C7−C8 bond distance increases from 1.400(19) to 1.444(18) Å. These values unanimously reveal a high-spin (hs) Co^{II} ion and a full 3,5-$DBSq^{\bullet-}$ ligand.[25,37] So, we can conclude that complex **1** has shown a VT transition from ls-[Co^{III}(3,5-DBCat)(3,5-DBSq)(bpe)] to hs-[Co^{II}(3,5-$DBSq)_2$(bpe)] with increasing temperature.

Complex **2**·*S* possesses the same 1D structure as that of **1**·*S*, except that the bridging ligand bpe in **1**·*S* has been replaced with azpy (Figure 2b). At 100 K, the dioxolene ligand in the asymmetric unit is also occupied by a "half" 3,5-$DBCat^{2-}$ and a "half" 3,5-$DBSq^{\bullet-}$, and the 1D chain is in the ls-Co^{III}−Cat^{2-}-$Sq^{\bullet-}$ state. Upon warming, the amplitude of the temperature-dependent variations in the Co−O, Co−N, C−O, and C6−C7 distances keeps in step with that of **1**·*S*. So, **2**·*S* also remains in the ls-Co^{III}−Cat^{2-}-$Sq^{\bullet-}$ state below room temperature. As for the desolvated complex **2**, the VT transition may be expectable

dx.doi.org/10.1021/ic502471v | *Inorg. Chem.* 2014, 53, 13212−13219

due to the isoelectric nature of azpy and bpe. As shown in Table 2b, when the temperature rises from 100 to 300 K, the Co−O, Co−N, and C6−C7 bond lengths have increased by 0.164 Å (average), 0.148 Å, and 0.040 Å, respectively, while the C−O bond lengths decrease to 1.278 Å. So, an expected interconversion between the two tautomers, that is, ls-[Co^{III}(3,5-DBCat)(3,5-DBSq)(azpy)] and hs-[Co^{II}(3,5-$DBSq)_2$(azpy)], was observed.

Complex **3**·*S* crystallizes in the triclinic space group $P\bar{1}$, the asymmetric unit contains two crystallographically independent cobalt ions, and the two different 1D chains possessing these cobalt ions are denoted as **Mol1** (Co1) and **Mol2** (Co2), respectively. As shown in Figure 3, Co1 and Co2 ions locate in

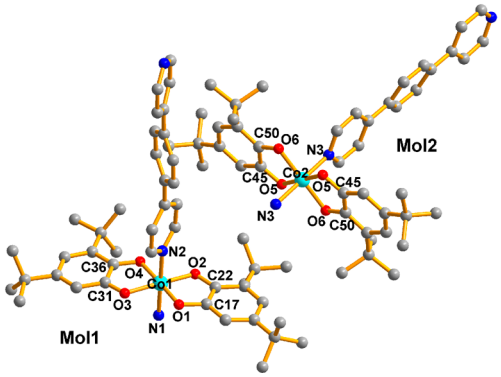

Figure 3. Two different structural units in **3**·*S* shown with selected atom labels. Hydrogen atoms and solvent molecules were omitted for clarity.

similar coordination geometry, but Co2 ion sits on an inversion center. For **Mol1**, the Co1−O and Co1−N bond lengths at 100 K lie in the ranges of 1.858(5)−1.904(5) and 1.921(6)−1.939(6) Å, respectively, implying that Co1 is an ls-Co^{III} ion. Because the two dioxolene ligands around Co1 ion are crystallographically distinguished, we can speculate that they must be a Cat^{2-} and an $Sq^{\bullet-}$, respectively. By scrutinizing Table 2a, we can find that the C17−O1, C22−O2, and C17−C22 bond lengths are 1.343(8), 1.335(9), and 1.417(9) Å, respectively, while the C31−O3, C36−O4, and C31−C36 bond lengths are 1.265(9), 1.299(8), and 1.468 (10) Å, which clearly indicates that the dioxolene ligand containing O1 and O2 is 3,5-$DBCat^{2-}$ and which, with O3 and O4, is 3,5-$DBSq^{\bullet-}$, respectively. While for **Mol2**, the Co−O, Co−N, C−O, and C45−C50 bond lengths at 100 K resemble those of **1**·*S* and **2**·*S* (Table 2a), and because Co2 ion locates on an inversion center, the dioxolene ligand (containing O5 and O6) can also be viewed as a "mixture" of "half" 3,5-$DBCat^{2-}$ and "half" 3,5-$DBSq^{\bullet-}$. Therefore, both cobalt ions are in the ls-Co^{III} state at 100 K, and the two structural units display the ls-Co^{III}−Cat^{2-}-$Sq^{\bullet-}$ electronic configuration. At 300 K, the bond lengths of Co−O and Co−N in **Mol1** are 2.012(10)−2.057(9) and 2.046(10)−2.071(11) Å, respectively, suggesting that the cobalt ion has converted into hs-Co^{II}. On the other hand, the bond lengths of C−O decrease to 1.264(14)−1.295(13) Å, and the bond lengths of C17−C22 and C31−C36 increase to 1.454(15)−1.460(17) Å, respectively. These structural changes indicate that a VT transition has occurred in **Mol1**; that is, an intramolecular electron transfer from Cat^{2-} to ls-Co^{III} and consequent spin crossover of ls-Co^{II} to hs-Co^{II} occurred, thus forming the hs-Co^{II}-$(Sq^{\bullet-})_2$ room-temperature species. In contrast to **Mol1**, **Mol2** shows little changes in the structural parameters along with temperature increasing (Table 2a), which are similar to those of **1**·*S* and **2**·*S*, showing that **Mol2** remains in the ls-Co^{III}−Cat^{2-}-$Sq^{\bullet-}$ state. In other words, only one unit of complex **3**·*S* undergoes VT transition.

INFRARED SPECTROSCOPY

From the structural point of view, complexes **1**·*S* and **2**·*S* and their desolvated samples **1** and **2** display different electronic states at room temperature, that is, ls-Co^{III}−Cat^{2-}-$Sq^{\bullet-}$ for **1**·*S* and **2**·*S* and hs-Co^{II}-$(Sq^{\bullet-})_2$ for **1** and **2**, respectively. Thus, differences between their infrared spectra are imaginable, which are shown in Figure 4 in the region of 1650−1200 cm^{-1}. Because complexes **1**·*S* and **2**·*S* are analogues, only **1**·*S* is described here. At room temperature, the bands at 1437, 1411, and 1284 cm^{-1} are characteristic features of the catecholate ligand 3,5-$DBCat^{2-}$, while those at 1458 and 1355 cm^{-1} can be assigned to the semiquinonate ligand 3,5-$DBSq^{\bullet-}$,[38] which are coincident with the ls-Co^{III}−Cat^{2-}-$Sq^{\bullet-}$ species of **1**·*S* at 300 K. In the desolvated sample **1**, the ligand 3,5-$DBCat^{2-}$ has converted to ligand 3,5-$DBSq^{\bullet-}$ at 300 K; accompanying this conversion, the characteristic bands of catecholate (1437, 1411 and 1284) disappear, and the relative intensity of semiquinonate bands increases. So, although **1**·*S* itself can not undergo thermally induced VT transition near room temperature, a solvent-induced VT transition between **1**·*S* and **1** can be established.

MAGNETIC PROPERTIES

Magnetic susceptibilities χ_M of **1**·*S*−**3**·*S* were measured in two successive cooling/heating cycles in the 5−390 K temperature range under ambient pressure, and the corresponding $\chi_M T$ versus T plots are shown in Figure 5. At the beginning, the three samples were cooled from 300 to 5 K and then heated from 5 to 390 K, which is the first cycle (300 → 5→390 K), showing solvent-dependent magnetic behaviors, and then the

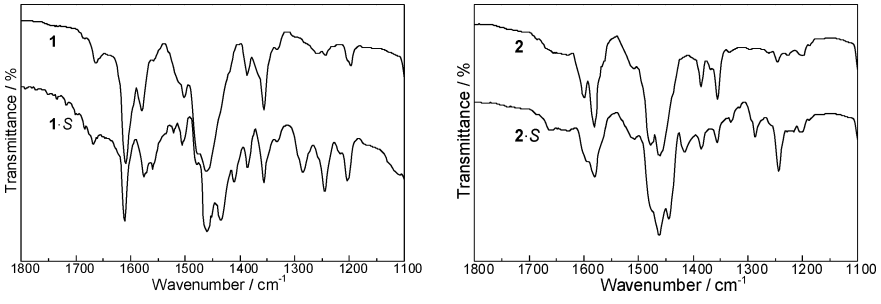

Figure 4. Infrared spectra of complexes **1**·*S* and **1** (left), **2**·*S* and **2** (right) between 1100 and 1800 cm^{-1}.

dx.doi.org/10.1021/ic502471v | Inorg. Chem. 2014, 53, 13212−13219

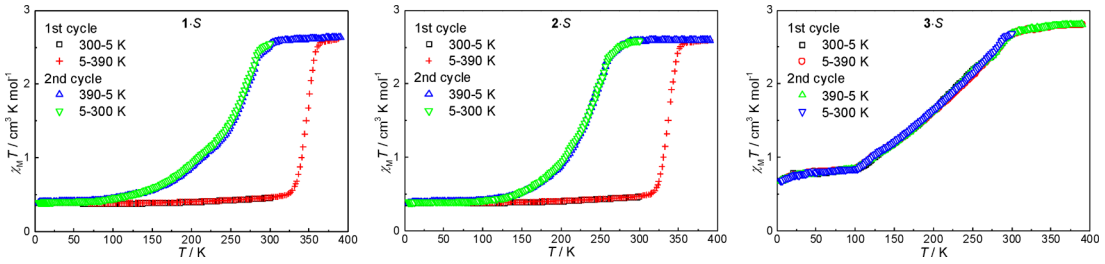

Figure 5. $\chi_M T$ versus T plots of **1**·*S*–**3**·*S* and **1**–**3** (per Co unit for **1**·*S* and **2**·*S*; per $Co_{1.5}$ unit for **3**·*S*). Applied field: 5000 Oe.

samples were cooled from 390 to 5 K and subsequently heated to 300 K, which is the second cycle (390 → 5→300 K), showing thermally induced VT transitions. Because **1**·*S* (and **1**) displays the same magnetic properties as those of **2**·*S* (and **2**), we will discuss **1**·*S* and **1** here. In the first cycle, the $\chi_M T$ value of **1**·*S* slightly decreases from 0.46 to 0.39 cm^3 K mol^{-1}, a value close to the paramagnetic free radical 3,5-$DBSq^{\bullet-}$,[39,40] which is in consistent with the ls-Co^{III}–Cat^{2-}-$Sq^{\bullet-}$ electronic configuration of **1**·*S* at temperature below 300 K that has been revealed by X-ray diffraction studies. As the compound warms, the $\chi_M T$ value first recovers, then rises abruptly from 0.52 cm^3 K mol^{-1} at 325 K to 2.58 cm^3 K mol^{-1} at 370 K ($T_{1/2}$ = 348 K), corresponding to the formation of hs-Co^{II}–$Sq^{\bullet-}$-$Sq^{\bullet-}$ species. Because the lattice solvent molecules begin to escape at 310 K and completely escape at 370 K (Figure S1, Supporting Information), respectively, the abrupt increase of the $\chi_M T$ value can be attributed to the conversion from **1**·*S* to **1**, that is, from ls-[Co^{III}(3,5-DBCat)(3,5-DBSq)(bpe)]·$2CH_3CN$·$2H_2O$ to hs-[Co^{II}(3,5-$DBSq)_2$(bpe)]. This conversion is apparently triggered by the rapid loss of solvent molecules, which may induce steric hindrance and/or strong hydrogen bonds that prevent the expansion of the 1D chain structure associated with VT transition.[41−45] In the successive second cycle, the solvent-free sample **1** remains in the hs-Co^{II}–$Sq^{\bullet-}$-$Sq^{\bullet-}$ state upon cooling from 390 to 300 K; then, the $\chi_M T$ value decreases gradually from 2.53 cm^3 K mol^{-1} at 300 K to 0.42 cm^3 K mol^{-1} at 77 K ($T_{1/2}$ = 253 K), clearly suggesting a VT transition from hs-Co^{II}–$Sq^{\bullet-}$-$Sq^{\bullet-}$ to ls-Co^{III}–Cat^{2-}-$Sq^{\bullet-}$. When the temperature increases from 5 to 300 K, the $\chi_M T$ values completely overlap those of cooling mode (390 to 5 K). So, a reversible, thermally induced VT transition of hs-Co ^{II}-$Sq^{\bullet-}$-$Sq^{\bullet-}$ ↔ ls-Co^{III}–Cat^{2-}-$Sq^{\bullet-}$ is achieved.

The $\chi_M T$ value of **3**·*S* is 2.68 cm^3 K mol^{-1} at 300 K, which is less than the theoretic one expected for the hs-Co^{II}–$Sq^{\bullet-}$-$Sq^{\bullet-}$ (**Mol1**) and (ls-Co^{III}–Cat^{2-}-$Sq^{\bullet-}$)$_{0.5}$ (**Mol2**) components in **3**·*S*. As the material cools, the $\chi_M T$ value shows a linear decrease to 0.84 cm^3 K mol^{-1} at 100 K and then gradually to 0.68 cm^3 K mol^{-1} at 5 K, which reveals that **Mol1** has converted to its tautomer ls-Co^{III}–Cat^{2-}-$Sq^{\bullet-}$ ($T_{1/2}$ = 212 K), in complete agreement with the results obtained by single-crystal XRD studies. When the sample is heated to 390 K and then followed by the second temperature cycle, the $\chi_M T$ values of **3**·*S* and **3** are completely the same as each other, showing VT transitions that are solvent independent. We notice that **3**·*S* shows a different solvent effect from that of **1**·*S* or **2**·*S*, which may be due to different packing styles of 1D chains in **1**·*S* (**2**·*S*) and **3**·*S*. As shown in Figure S3 (Supporting Information), the 1D chains in **1**·*S* or **2**·*S* are packed in the parallel mode, while the two different 1D chains (**Mol1** and **Mol2**) in **3**·*S* are orthogonally packed, so that a more rigid supramolecular framework of **3** that is inert to solvent molecules is achieved.

We notice that the 1D structures in the desolvated forms, **1**–**3**, show thermally induced VT transitions with different transition temperatures ($T_{1/2}$). To find the key factor determining such temperature, we have compared their VT behaviors with that of the reported complex [Co^{III}(3,5-DBCat)(3,5-DBSq)(bipy)] (named as complex **4**) in the cooling process.[27] As shown in Figure 6 and Table 3, the

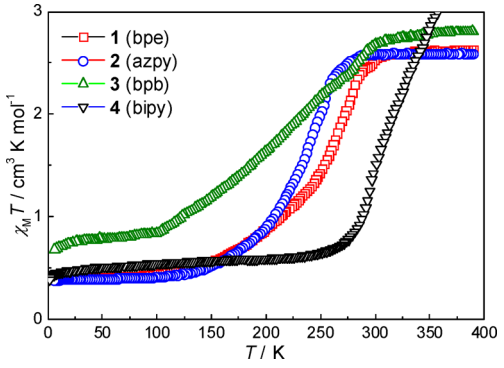

Figure 6. Comparison of VT transitions of complexes **1**–**4** in the cooling process. Applied field: 5000 Oe.

Table 3. VT Transition Temperatures of 1–4 in the 390–5 K Cooling Process

	1	2	3	4
bridging ligand	bpe	azpy	bpb	bipy
$T_{1/2}$/K	253	234	212	>330

$T_{1/2}$ value follows an order $T_{1/2}$(**3**) < $T_{1/2}$(**2**) < $T_{1/2}$(**1**) < $T_{1/2}$(**4**), which means that the ligand-field strength of bridging ligand in **1**–**4** shows the same sequence, that is, bpb < azpy < bpe < bipy. Because the four bridging ligands uniformly coordinate to Co ions with the pyridyl nitrogen atoms, the differences in ligand-field strengths should derive from the electronic nature of substituted groups −CH═CH−, −N═N−, and $-C_6H_4-$ in bpe, azpy, and bpb, respectively (Scheme 1). It is generally accepted that the substitute groups −CH═CH−, −N═N−, and $-C_6H_4-$ possess increasing electron-withdrawing abilities; thus, they could lower the electron density of pyridyl nitrogen atoms and result in decreasing ligand-field strengths. Therefore, the VT transition can only occur at lower temperature at $T_{1/2}$(**1**) > $T_{1/2}$(**2**) > $T_{1/2}$(**3**). Accordingly, complex **4** with bridging ligand bipy should have the strongest ligand-field strength among the four bridging ligands and definitely features the highest $T_{1/2}$ value.

PHOTOMAGNETIC PROPERTIES

Taking into account that complexes **1**·*S* and **2**·*S* show thermally induced VT transitions in their desolvated forms (**1** and **2**) and

dx.doi.org/10.1021/ic502471v | Inorg. Chem. 2014, 53, 13212−13219

3·*S* (and **3**) shows incomplete VT transition, we have investigated the photoeffects of **1**−**3** and found that only **1** underwent photoinduced VT transition. When sample **1** was irradiated with a green light for 3 h at 5 K (Figure 7), the $\chi_M T$

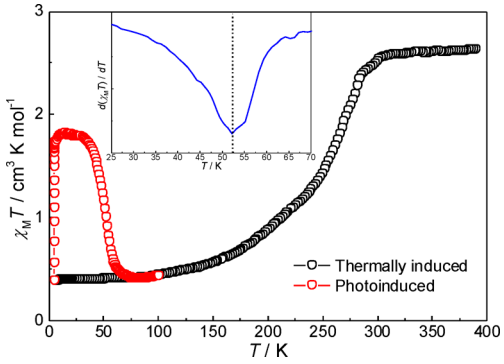

Figure 7. $\chi_M T$ versus T plot of **1** showing thermally and photoinduced VT transitions. Irradiation: 532 nm light of 150 mW at 5 K for 3 h; applied field: 5000 Oe. (inset) $d(\chi_M T)/dT$ versus T plot of the photoinduced magnetic susceptibility used to evaluate T_{LIESST}.

value significantly rose to 1.74 cm^3 K mol^{-1}, attaining ~60% of that at room temperature, clearly indicating that the 1D chain had undergone photoinduced charge transfer from Cat^{2-} to ls-Co^{III} and consequently spin crossover from ls-Co^{III} to hs-Co^{II}, that is, photoinduced VT transition. After light was switched off and the sample was warmed from 5 K at a sweeping rate of 0.5 K min^{-1}, the $\chi_M T$ value slightly increased to 1.83 cm^3 K mol^{-1} at 15 K and then gradually decreased to 0.42 cm^3 K mol^{-1} at 77 K, where the $\chi_M T$ value restored to that of the nonirradiated complex. The T_{LIESST} value (the critical temperature of light-induced excited spin state trapping) was identified as 52 K by the $d(\chi_M T)/dT$ versus T plot (Figure 7, inset).[46] This result indicates that the interconversion between ls-[Co^{III}(3,5-DBCat)(3,5-DBSq)(bpe)] and hs-[Co^{II}(3,5-$DBSq)_2$(bpe)] is photoswitchable.

As shown above, the photoinduced metastable state can be trapped at low temperature. To study the relaxation kinetics of metastable species, we performed the measurements at various temperatures. As shown in Figure 8a, the decay data are fitted using the stretched exponential decay model. The molar fraction of metastable state is defined from the equation $\gamma(t) = [(M(t) - M_{OFF})/(M(0) - M_{OFF})] \times 100$,[47,48] where $M(t)$ is the $\chi_M T$ value at time t after illumination, $M(0)$ is the $\chi_M T$ value at $t = 0$ when the light is switched off, and M_{OFF} is the $\chi_M T$ value before illumination. The relaxation rate constant can be evaluated by the equation $\gamma(t) = \gamma_0 \exp[-(K_{VT}(T)t)]^{\beta}$ valid for photomagnetic species,[49−51] where γ_0 is the converted fraction at $t = 0$, $K_{VT}(T)$ is the rate constant of VT relaxation at temperature T, t is the relaxation time, and β is a parameter accounting for the distribution of relaxation times. The plot of $\ln[K_{VT}(T)]$ versus $1/T$ (Figure 8b) shows two distinct relaxation regions, as observed in other photoinduced VT complexes.[25,29,36,51−53] In the low-temperature region (5−10 K), the relaxation is essentially temperature independent, while in the higher temperature region the thermally activated relaxation ($T \geq 20$ K) obeys the Arrhenius law; the best fit (β = 0.6) gives a thermal activation factor $K_{VT}^0 = 3.664 \times 10^{-2}$ s^{-1} and an activation energy $E_a = 99.68$ cm^{-1}, similar to those of cobalt VT complexes.[36,43,48,51]

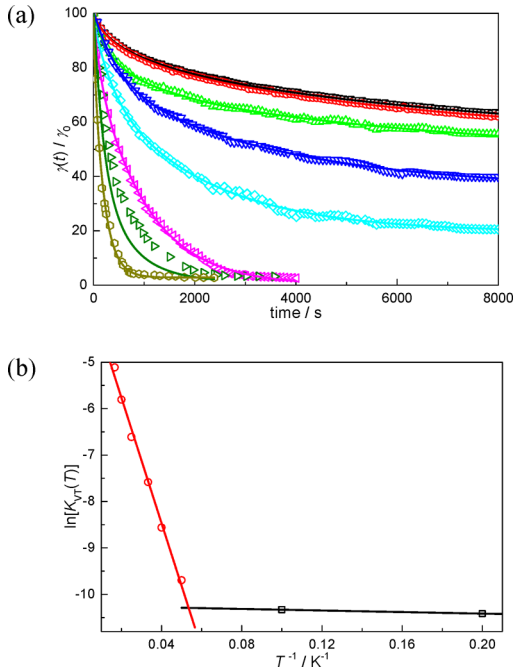

Figure 8. (a) Normalized relaxation of the photoinduced metastable state of **1** at 5 K (black), 10 K (red), 20 K (green), 25 K (blue), 30 K (cyan), 40 K (magenta), 50 K (olive), and 60 K (dark yellow). (b) The relaxation constants plotted as $\ln[K_{VT}(T)]$ vs T^{-1} with fitted lines in the two regions (black, 5−10 K; red, 20−60 K).

CONCLUSIONS

We have reported three 1D cobalt complexes, whose solid-state VT transition behaviors are tunable by solvent molecules, bridging pyridine ligands, temperature, and light. Complexes **1**·*S* and **2**·*S* reside in the ls-Co^{III}−Cat^{2-}-$Sq^{\bullet-}$ states below room temperature and display thermally induced complete VT transitions upon desolvation of solvent molecules, whereas complex **3**·*S* shows solvent-independent incomplete VT transition in whole temperature range. The difference in the solvent effects is assigned to the different packing structures of 1D chains between **1**·*S* (**2**·*S*) and **3**·*S*. On the other hand, the VT transition temperature shows an order of $T_{1/2}(\mathbf{3}) < T_{1/2}(\mathbf{2}) < T_{1/2}(\mathbf{1}) < T_{1/2}(\mathbf{4})$, coincident with the increasing ligand-field strength of bridging ligands. Meanwhile, the solvent-free complex **1** exhibits an efficient photoinduced VT transition, and the photoinduced metastable state undergoes thermally activated relaxation of magnetization.

ASSOCIATED CONTENT

Supporting Information

Crystallographic information in CIF format, TGA of **1**·*S*−**3**·*S*, details of "Squeeze" for complex **3**·*S*, tabulated bond angles, three-dimensional packing structures, $\chi_M T$ versus T plots, and IR spectra of studied compounds. This material is available free of charge via the Internet at http://pubs.acs.org. CCDC 1023735, 1023736, 1006400, 1006401, 1012420, and 1017385−1017389 contain the supplementary crystallographic data, which can be obtained free of charge from the Cambridge Crystallographic Data Center via www.ccdc.cam.ac.uk/data_request/cif.

dx.doi.org/10.1021/ic502471v | Inorg. Chem. 2014, 53, 13212−13219

AUTHOR INFORMATION

Corresponding Author

*E-mail: taojun@xmu.edu.cn.

Notes

The authors declare no competing financial interest.

ACKNOWLEDGMENTS

This work was supported by the National Natural Science Foundation of China (Grant No. 21325103), the National Key Basic Research Program of China (No. 2014CB845601), and the Specialized Research Fund for the Doctoral Program of Higher Education (Grant No. 20110121110012).

REFERENCES

(1) Kahn, O.; Kröber, J.; Jay, C. *Adv. Mater.* **1992**, *4*, 718−728.
(2) Sato, O.; Iyoda, T.; Fujishima, A.; Hashimoto, K. *Science* **1996**, *272*, 704−705.
(3) Miller, J. S. *Inorg. Chem.* **2000**, *39*, 4392−4408.
(4) Dei, A.; Gatteschi, D.; Sangregorio, C.; Sorace, L. *Acc. Chem. Res.* **2004**, *37*, 827−835.
(5) Evangelio, E.; Ruiz-Molina, D. *Eur. J. Inorg. Chem.* **2005**, *2005*, 2957−2971.
(6) Kepert, C. J. *Chem. Commun.* **2006**, *42*, 695−700.
(7) Sato, O.; Tao, J.; Zhang, Y.-Z. *Angew. Chem., Int. Ed.* **2007**, *46*, 2152−2187.
(8) Wang, M.-S.; Guo, G.-C.; Zou, W.-Q.; Zhou, W.-W.; Zhang, Z.-J.; Xu, G.; Huang, J.-S. *Angew. Chem., Int. Ed.* **2008**, *47*, 3565−3567.
(9) Zhang, Z.-J.; Xiang, S.-C.; Guo, G.-C.; Xu, G.; Wang, M.-S.; Zou, J.-P.; Guo, S.-P.; Huang, J.-S. *Angew. Chem., Int. Ed.* **2008**, *47*, 4149−4152.
(10) Wang, M.-S.; Xu, G.; Zhang, Z.-J.; Guo, G.-C. *Chem. Commun.* **2010**, *46*, 361−376.
(11) Xu, G.; Guo, G.-C.; Guo, J.-S.; Guo, S.-P.; Jiang, X.-M.; Yang, C.; Wang, M.-S.; Zhang, Z.-J. *Dalton Trans.* **2010**, *39*, 8688−8692.
(12) Buchanan, R. M.; Pierpont, C. G. *J. Am. Chem. Soc.* **1980**, *102*, 4951−4957.
(13) Pierpont, C. G. *Coord. Chem. Rev.* **2001**, *216−217*, 99−125.
(14) Adams, D. M.; Dei, A.; Rheingold, A. L.; Hendrickson, D. N. *Angew. Chem., Int. Ed.* **1993**, *32*, 880−882.
(15) Gütlich, P.; Dei, A. *Angew. Chem., Int. Ed.* **1997**, *36*, 2734−2736.
(16) Sato, O.; Hayami, S.; Gu, Z.-Z.; Takahashi, K.; Nakajima, R.; Fujishima, A. *Chem. Phys. Lett.* **2002**, *355*, 169−174.
(17) Carbonera, C.; Dei, A.; Létard, J.-F.; Sangregorio, C.; Sorace, L. *Angew. Chem., Int. Ed.* **2004**, *43*, 3136−3138.
(18) Li, B.; Yang, F.-L.; Tao, J.; Sato, O.; Huang, R.-B.; Zheng, L.-S. *Chem. Commun.* **2008**, *44*, 6019−6021.
(19) Dai, J.; Kanegawa, S.; Li, Z.; Kang, S.; Sato, O. *Eur. J. Inorg. Chem.* **2013**, *2013*, 4150−4153.
(20) Pierpont, C. G.; Buchanan, R. M. *Coord. Chem. Rev.* **1981**, *38*, 45−87.
(21) Adams, D. M.; Hendrickson, D. N. *J. Am. Chem. Soc.* **1996**, *118*, 11515−11528.
(22) Sato, O.; Hayami, S.; Gu, Z.-Z.; Seki, K.; Nakajima, R.; Fujishima, A. *Chem. Lett.* **2001**, *30*, 874−875.
(23) Adams, D. M.; Dei, A.; Rheingold, A. L.; Hendrickson, D. N. *J. Am. Chem. Soc.* **1993**, *115*, 8221−8229.
(24) Sato, O.; Cui, A.; Matsuda, R.; Tao, J.; Hayami, S. *Acc. Chem. Res.* **2007**, *40*, 361−369.
(25) Beni, A.; Dei, A.; Laschi, S.; Rizzitano, M.; Sorace, L. *Chem.—Eur. J.* **2008**, *14*, 1804−1813.
(26) Jung, O.-S.; Pierpont, C. G. *J. Am. Chem. Soc.* **1994**, *116*, 2229−2230.
(27) Imaz, I.; Maspoch, D.; Rodríguez-Blanco, C.; Pérez-Falcón, J. M.; Campo, J.; Ruiz-Molina, D. *Angew. Chem., Int. Ed.* **2008**, *47*, 1857−1860.
(28) Chen, L.-Q.; Wei, R.-J.; Tao, J.; Huang, R.-B.; Zheng, L.-S. *Sci. China Chem.* **2012**, *55*, 1037−1041.
(29) Affronte, M.; Beni, A.; Dei, A.; Sorace, L. *Dalton Trans.* **2007**, *43*, 5253−5259.
(30) Li, B.; Chen, L.-Q.; Wei, R.-J.; Tao, J.; Huang, R.-B.; Zheng, L.-S.; Zheng, Z. *Inorg. Chem.* **2010**, *50*, 424−426.
(31) Altomare, A.; Burla, M. C.; Camalli, M.; Cascarano, G. L.; Giacovazzo, C.; Guagliardi, A.; Moliterni, A. G. G.; Polidori, G.; Spagna, R. *J. Appl. Crystallogr.* **1999**, *32*, 115−119.
(32) Spek, A. L. *Acta Crystallogr., Sect. D* **2009**, *65*, 148−155.
(33) Boone, S. R.; Purser, G. H.; Chang, H. R.; Lowery, M. D.; Hendrickson, D. N.; Pierpont, C. G. *J. Am. Chem. Soc.* **1989**, *111*, 2292−2299.
(34) Brese, N. E.; O'Keeffe, M. *Acta Crystallogr., Sect. B* **1991**, *47*, 192−197.
(35) Mulyana, Y.; Nafady, A.; Mukherjee, A.; Bircher, R.; Moubaraki, B.; Murray, K. S.; Bond, A. M.; Abrahams, B. F.; Boskovic, C. *Inorg. Chem.* **2009**, *48*, 7765−7781.
(36) Li, B.; Tao, J.; Sun, H.-L.; Sato, O.; Huang, R.-B.; Zheng, L.-S. *Chem. Commun.* **2008**, *44*, 2269−2271.
(37) Tao, J.; Maruyama, H.; Sato, O. *J. Am. Chem. Soc.* **2006**, *128*, 1790−1791.
(38) Patricia, T. T.; Sandra, M. V.; Manuela, L.; Andrea, L.; Paolo, F.; Andrea, D.; Roberto, R. *Phys. Chem. Chem. Phys.* **2012**, *14*, 1038−1047.
(39) Li, B.; Yang, F.-L.; Tao, J.; Sato, O.; Huang, R.-B.; Zheng, L.-S. *Chem. Commun.* **2008**, *44*, 6019−6021.
(40) Alley, K. G.; Poneti, G.; Robinson, P. S. D.; Nafady, A.; Moubaraki, B.; Aitken, J. B.; Drew, S. C.; Ritchie, C.; Abrahams, B. F.; Hocking, R. K.; Murray, K. S.; Bond, A. M.; Harris, H. H.; Sorace, L.; Boskovic, C. *J. Am. Chem. Soc.* **2013**, *135*, 8304−8323.
(41) Neville, S. M.; Halder, G. J.; Chapman, K. W.; Duriska, M. B.; Southon, P. D.; Cashion, J. D.; Létard, J.-F.; Moubaraki, B.; Murray, K. S.; Kepert, C. J. *J. Am. Chem. Soc.* **2008**, *130*, 2869−2876.
(42) Southon, P. D.; Liu, L.; Fellows, E. A.; Price, D. J.; Halder, G. J.; Chapman, K. W.; Moubaraki, B.; Murray, K. S.; Létard, J.-F.; Kepert, C. J. *J. Am. Chem. Soc.* **2009**, *131*, 10998−11009.
(43) Mulyana, Y.; Poneti, G.; Moubaraki, B.; Murray, K. S.; Abrahams, B. F.; Sorace, L.; Boskovic, C. *Dalton Trans.* **2010**, *39*, 4757−4767.
(44) Chen, X.-Y.; Shi, H.-Y.; Huang, R.-B.; Zheng, L.-S.; Tao, J. *Chem. Commun.* **2013**, *49*, 10977−10979.
(45) Chen, X.-Y.; Huang, R.-B.; Zheng, L.-S.; Tao, J. *Inorg. Chem.* **2014**, *53*, 5246−5252.
(46) Létard, J.-F.; Capes, L.; Chastanet, G.; Moliner, N.; Létard, S.; Real, J.-A.; Kahn, O. *Chem. Phys. Lett.* **1999**, *313*, 115−120.
(47) Létard, J.-F.; Guionneau, P.; Rabardel, L.; Howard, J. A. K.; Goeta, A. E.; Chasseau, D.; Kahn, O. *Inorg. Chem.* **1998**, *37*, 4432−4441.
(48) Cui, A.; Takahashi, K.; Fujishima, A.; Sato, O. *J. Photochem. Photobiol., A* **2004**, *167*, 69−73.
(49) Chamberlin, R. V.; Mozurkewich, G.; Orbach, R. *Phys. Rev. Lett.* **1984**, *52*, 867−870.
(50) Carbonera, C.; Dei, A.; Sangregorio, C.; Létard, J.-F. *Chem. Phys. Lett.* **2004**, *396*, 198−201.
(51) Carbonera, C.; Dei, A.; Létard, J.-F.; Sangregorio, C.; Sorace, L. *Inorg. Chim. Acta* **2007**, *360*, 3825−3828.
(52) Beni, A.; Dei, A.; Rizzitano, M.; Sorace, L. *Chem. Commun.* **2007**, *43*, 2160−2162.
(53) Dapporto, P.; Dei, A.; Poneti, G.; Sorace, L. *Chem.—Eur. J.* **2008**, *14*, 10915−10918.